Chapter 9

IONOSPHERIC PHYSICS

Section 9.1 F.J. Rich
Section 9.2 F.J. Rich
Section 9.3 Su. Basu

9.1 STRUCTURE OF THE IONOSPHERE

9.1.1 Ionospheric Layers

The ionized atmosphere of the earth is composed of a series of overlapping layers. In each layer there is an altitude of maximum density, above and below which the ionization density tends to drop off. The total ionization profile with the layers indicated is shown in Figure 9-1. Characteristics of the layers are shown in Table 9-1. This profile is valid only for midlatitudes. In the equatorial region, the profile is distorted by the geomagnetic field, and in the polar region, the profile is distorted by ionization by energetic particles, magnetospheric coupling, and other effects.

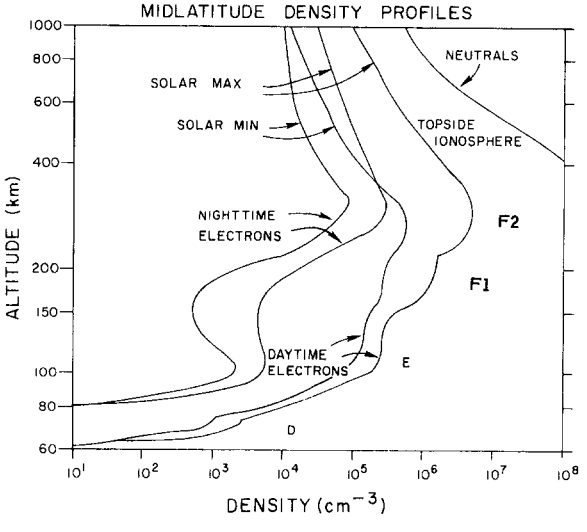

Figure 9-1. Total ionization profile with ionospheric layers.

The *D region* is present only during daylight hours. The altitude of the peak density is normally around 90 km, but this may decrease considerably to ~ 78 km when the solar x-ray flux is enhanced. The *E region* peak density occurs at a peak altitude of 110 km. At sunset, the E Region electron density drops by a factor of 10 or more in a short period (tens of minutes) before reaching a nighttime equilibrium density. At night, the region of low density near 150 km between the E region and the F region may have a sharply lower density than shown in Figure 9-1 or the density may be great enough so that there is no depletion region depending on geophysical conditions. The *F region* is a combination of two somewhat different regions. The *F1 region* has an altitude peak near 200 km, but is absent at night. The *F2 region* has a peak near 300 km during the day and at higher altitudes at night. Shortly after sunset, the absolute density near the peak of the F region often increases due to plasma transport processes before decreasing to a night time value.

The *Topside Ionosphere* is the name given to the rest of the ionosphere above the F region peak. In a simple model of the ionosphere, the density of the topside ionosphere decreases exponentially with height with some char-

Table 9-1. Layers of daytime midlatitude ionosphere.

Layer	Altitude(km)	Major Component	Production Cause
D	70–90 km	NO^+, O_2^+	Lyman Alpha, x-rays
E	95–140 km	O_2^+, NO^+	Lyman Beta, Soft x-rays, UV Continuum
F1	140–200 km	O^+, NO^+	He II, UV Continuum (100–800Å)
F2	200–400 km	O^+, N^+	He II, UV Continuum (100–800Å)
Topside F	> 400 km	O^+	Transport from Below
Plasmasphere	> 1200 km	H^+	Transport from Below

acteristic scale height until the ionization density is below detectable levels. In the mid and low latitude ionosphere, the geomagnetic field tends to trap ions, especially hydrogen ions, that would otherwise drift off into deep space. Thus, somewhere between 800 and 2000 km altitude the scale height increases to a very large value ($\geq$ one earth radius). If one follows a geomagnetic field line out to the equatorial plane and back into the conjugate ionosphere, the density would change by less than 10^2 and in some cases less than 10. This region of trapped ionospheric ions is the *Plasmasphere* [Carpenter and Park, 1973]. The outer edge of the plasmasphere where ionospheric ions are not trapped is the *Plasmapause*. The plasmapause is located approximately along the geomagnetic field line that maps down to 60° magnetic latitude. A representation of the topside ionosphere and plasmasphere is shown in Figure 9-2.

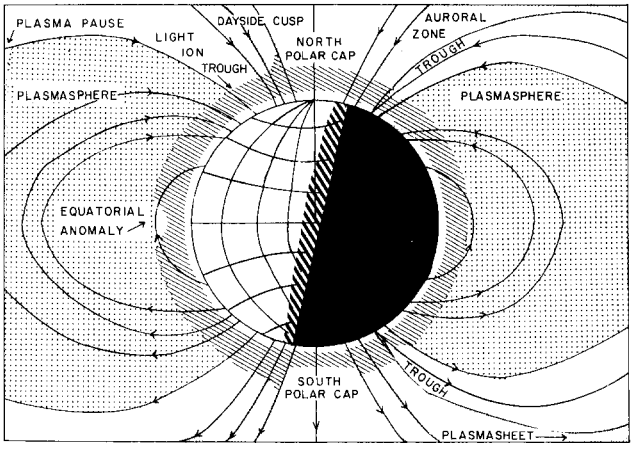

Figure 9-2. Representation of topside ionosphere and plasmasphere

For further information about ionospheric layers see Banks and Kockarts [1973]; Kohnlein [1978]; and Chapters 12 and 21.

9.1.2 Chapman Theory for Ionospheric Layers

The layering of the ionosphere was first discussed by Sydney Chapman in the 1920s. Ionizing photons from the sun will produce more and more ions as they penetrate deeper and deeper into an atmosphere with rapidly increasing density. As photoionization occurs, the flux of photons is attenuated until a depth is reached that photoionization production drops. Thus, a layer of ionization near the altitude of maximum production is created.

The process of quantitatively determining the height profile of ionization is outlined as follows. We assume that direct photoionization and recombination are the only sources of production and loss respectively. We can find the ion density at a height h due to a single frequency of ionizing photons ν by setting the production rate equal to the loss rate for a quasi-equilibrium ionosphere. The production rate is

$$Q_\nu(h) = \beta_\nu N(h) F_\nu(h) \text{ ionizations cm}^{-3} \text{ s}^{-1} \quad (9.1)$$

where β_ν is the absorption cross section for photoionization, N(h) is the neutral density at the height h, and $F_\nu(h)$ is the photon flux of frequency ν. The recombination rate is approximately

$$L_\nu(h) = \alpha_R N_i N_e \quad (9.2)$$

where α_R is the recombination coefficient and N_i and N_e are the ion and electron densities. If multiply charged and negative ions are not important, $N_i = N_e$. For an appropriate set of assumptions, the density near the peak of the layer is

$$N_e(h) \approx \left(\frac{Q^M}{\alpha_R}\right)^{1/2} \left[1 - \frac{(h-h_m)^2}{4H^2}\right] \quad (9.3)$$

where Q_M is the production at the peak of the layer, h_m is the height of the layer and H is the scale height of the neutral atmosphere. The parabolic variation of density with h around the peak gives the layers of the ionosphere their characteristic shape.

In principle, the above equation needs to be summed over all appropriate frequencies of incident photons to obtain the total ionospheric profile. In fact, many details about ionospheric chemistry (especially in the D and E layers) and about plasma transport (especially in the F layer) must be considered. For example, NO is not a significant component of the neutral atmosphere, but NO^+ is a significant ion component due to a chain of chemical reactions induced by photoionization. Details about computing an ionospheric model with all factors included is given by Banks and Kockarts [1973].

9.1.3 Ionization Production, Loss and Vertical Transport

Ionization production is generally a two-step process. The first step is the creation of ions from the neutrals by solar photons in the ultraviolet and x-ray spectrum, and to a lesser degree by collisions with energetic particles. Most of the ionization is produced by solar radiation with wavelengths less than 1026 Å, which ionizes O, O_2, and N_2. There are a vast array of minor constituents, especially molecular and metallic ions, that are important in understanding the ionosphere. Some of these minor constituents play important roles in the absorption of solar UV radiation (especially in the D region), in the production of airglow, in the chemistry of the ionosphere, and in the role of tracers to indicate ionospheric and atmospheric transport. A review

of photoionization is given by Hudson [1971] and Stolarski and Johnson [1972].

The second step in the creation of the ionosphere is the reaction between ions, neutrals, and electrons to create different forms of ionization than that created by direct ionization. Ionospheric chemistry explains why NO^+ is an important ionospheric ion despite the low abundance of NO in the neutral atmosphere. Two of the major reactions in the ionosphere which create NO^+ are

$$\begin{aligned} N_2 + O^+ &\rightarrow NO^+ + N \\ N_2^+ + O &\rightarrow NO^+ + N \end{aligned} \qquad (9.4)$$

All of the major reactions are summarized in Figure 9-1 of Torr [1979]. The reactions that result in minor constituents are quite numerous and not all of them are well understood. Reactions that should be mentioned involve metastable atomic states, negative ions, ionization by photoelectrons, energetic neutrals and vibrational states of molecules. Further details of ionospheric chemistry are given in Chapter 21.

After recombination of ions and electrons to form neutrals, the atoms are often in an excited state that is metastable. On the ground, such states are de-excited through collisions, but with the lower collision frequency in the thermosphere, forbidden atomic transitions occur which release photons not generally seen in the laboratory such as the 5577 Å and 6300 Å emissions of atomic oxygen.

Negative ions are generally found in the D and lower E regions. They are formed primarily through electron-neutral molecule collisions. Photodissociation of electrons from negative ions provides the major source of D-region electrons shortly after sunrise. See Ferguson [1971] and Turco [1974] for a discussion of D-region chemistry.

After electrons are removed from an atom by photoionization, they have an energy that depends upon the work function of the atom and the energy of the photon. The energy distribution function of photoelectrons is a complex function [Jasperse, 1977 and Doering et al., 1976] that can crudely be approximated by a combination of 2 eV and a 20 eV Maxwellian distribution. In the D and E regions, the photoelectrons lose their energy through collisions close to the location of their formation. In the F region, the photoelectrons can travel significant vertical distances before losing all of their energy. As a rule of thumb, photoelectrons traveling upward at altitudes above 300 km are considered as escaping because of the low collision frequency. Except in the polar regions, these photoelectrons do not truly escape but follow magnetic field lines into the opposite hemisphere. Some of their energy is lost to plasma in the plasmasphere and the rest is used to heat and populate the opposite ionosphere [Mantas et al. 1978]. Photoelectrons from the opposite hemisphere are most important when one hemisphere is in darkness and the other in sunlight.

Charge exchange reactions such as

$$O^+ + H \leftrightarrows O + H^+ \qquad (9.5)$$

are important to the dynamics of the ionosphere, especially above the density peak of the F region. Energetic ions can undergo a charge exchange process, cross magnetic field lines as a neutral and be re-ionized by a second charge exchange. The result is a transfer of energy across field lines that otherwise would be impossible.

The principal loss of ionization comes from recombination. This is simply the reaction of positive ions and electrons to form neutrals. The most important recombination reactions are

$$\begin{aligned} NO^+ + e^- &\rightarrow N + O \\ O_2 + e^- &\rightarrow O + O. \end{aligned} \qquad (9.6)$$

The charge exchange reaction

$$O^+ + O_2 \rightarrow O_2^+ + O \qquad (9.7)$$

is important to facilitate the recombination process. The major problem related to loss of ionization is not a lack of knowledge of the reactions but a lack of precise knowledge about the reaction rates. Reaction rates depend upon the density of the ions and neutrals, the atomic state of the incident and resultant ions, the vibrational state of molecules, and the temperature of the ions and electrons. If one reaction rate for any related part of the recombination process is not known precisely, it is difficult to determine the reaction rate of the complete recombination process. Solar eclipse data have been used to empirically determine some of the effective recombination rates. The knowledge of reaction rates for both production and loss covers a vast array of atomic and molecular reactions [Torr, 1979; Ferguson, 1971; and *DNA Rate Book*, 1972] known with varying degrees of precision.

Vertical transport of ions and electrons is principally governed by collision frequency and gravity. Below 130 km, the collision frequency of ions and electrons is so large that to a good approximation no ions or electrons enter or leave a unit volume. The unit volume may move up or down under the influence of pressure gradients. Between 130 km and 300 km the mean free path of electrons, and to a lesser degree ions, becomes comparable or larger than the scale height or layer thickness of the ionosphere. Diffusion becomes an important factor in plasma transport and energy exchange. Above an altitude of 300–400 km, the plasma can be treated as collisionless for many purposes. At high and midlatitudes, vertical transport is approximately along magnetic field lines and particles will tend to diffuse upward or downward according to their mass. Because the ions and electrons are electrically coupled, ambipolar diffusion must be considered. The ions and electrons diffuse upward together at a rate that must be less than a neutral particle with the mass of an electron and slightly greater than a neutral particle with the mass of the ion. Near the equator, vertical transport is impeded by the magnetic field lines. In the daytime, however, due to electrodynamic effects ionization

is transported upwards at the magnetic equator which subsequently diffuses down magnetic field lines at ± 15° magnetic latitudes. This results in the Appleton anomaly as discussed in greater detail in Section 9.2.2.4.

9.1.4 Neutral Winds and Horizontal Transport

Below 130 km altitude, the ion-neutral collision frequency is so high that ions will freely flow across field lines with the neutrals but the electrons are relatively fixed with respect to the magnetic field. As a result, neutral winds tend to cause ionospheric currents. These ionospheric currents are detected on the ground by the diurnal variations in the magnetic field at mid and low latitudes (+60° to −60°). The Sq (solar quiet) current system and the equatorial electrojet are the major current systems related to the neutral winds. The separation of ions and electrons in the E region produce polarization electric fields that can cause E × B drift of plasma in both the E- and F-regions [Evans, 1978].

Neutral winds are predominantly atmospheric tides with periods of 24, 12, 8, 6, . . . hours. The zero order neutral wind consists of a steady flow away from ~ 1400 local time toward ~ 0200. The latitude of these high and low pressure zones shifts seasonally with the sun. At high latitudes the neutral winds are strongly affected by geomagnetic activity [Roble et al., 1981]. The ring current, which causes the negative Dst midlatitude deflection is dissipated in the ionosphere near 60° which, in turn, heats the thermosphere. The Joule heating of the auroral zones and polar caps and the heating from precipitating particles also cause the high latitude thermosphere to be heated. As a result of the heating of the thermosphere, the neutral winds at high and midlatitudes can be strongly affected and even reverse direction.

The convection electric fields imposed upon the high latitude ionosphere from the magnetosphere also cause horizontal plasma transport. In the winter ionosphere, the drifts driven by the convection electric field are a major source of ionization in the polar cap drawing from the auroral zone and the dayside [Sojka et al., 1981]. The convection electric field can also decrease ionization by enhancing the recombination rates as ions are driven through the neutrals.

9.2 HIGH LATITUDE PHENOMENA

9.2.1 Total Ionization Trough and Light Ion Trough.

The total ionization trough is a region of decreased F-region ionization and/or total electron content found in a latitudinally narrow band near 60°–65° magnetic latitude [Ahmed et al., 1979]. The ends of the trough are typically found an hour after sunset and an hour before sunrise. The contour of the trough follows the contours of the auroral oval instead of paralleling the magnetic latitudes. As the auroral oval moves poleward, the trough moves poleward and expands in width. As the auroral oval moves equatorward, the trough moves equatorward and decreases in width. The depth of the trough (the ratio of minimum density to the density a few degrees equatorward and/or poleward) is typically a factor of ten in density or total electron content (TEC) but may vary from barely discernible to a factor of 10^3.

The equatorward wall of the trough tends to be found on the same field line or 1°–2° poleward of the plasmapause. From this observation has come the suggestion that the trough is formed by plasma flow upwards into evacuated flux tubes. The region equatorward lies on filled flux tubes that can replenish the plasma, and the region poleward of the trough is replenished by ionization induced by precipitating energetic particles. An alternate explanation is that the trough is created by the cancellation of the corotation and convection electric field in the evening sector. Plasma remains nearly stationery for several hours; depletion is due to recombination. After leaving the stagnation zone, the trough is sustained through the night by the lack of production in the region of the trough.

The light ion trough is a sharp drop in H^+ and He^+ density near the peak of F region and in the topside ionosphere. On the night side, the light ion trough or density gradient is collocated with the equatorward wall of the total ion trough. On the dayside, the light ion trough continues to be found near 60° magnetic latitude while the total ion trough either ceases to exist or moves to higher latitudes. For a satellite traveling in the altitude range from ~800 to ~1500 km on the dayside and ~600 to ~1500 km on the night side, the light ion trough is seen as a rapid transition between H^+ and O^+ as the dominant ion [Titheridge, 1976]. Above ~1500 km, the O^+ density is so low even when it is the dominant ion that the total density drops by a factor of ~10 to >10^3 at all local times at the same latitude as the light ion trough.

The plasma temperature in the F region near the trough and the equatorward wall of the auroral zone is increased substantially from the temperature in adjacent regions. This is partly related to energy from the ring current in the equatorial plane of the magnetosphere being transferred to the ionosphere. When this energy deposition is large enough, the airglow is enhanced to form stable auroral red (SAR) arcs. SAR arcs are generally subvisual. They tend to be most intense following a major geomagnetic storm.

9.2.2 The Ionosphere in the Auroral Oval.

We have known of the visual displays called auroras for centuries and we have known for the past century that auroras are associated with electromagnetic disturbances. However, it has only been since the start of the space age

we have known auroras are global and are the projection of activity at great altitudes in the magnetosphere and solar wind (Chapters 3 and 8). The global nature of auroras is generally acknowledged by referring to the auroral oval, a band a few degrees in latitude and around both magnetic poles where auroral phenomena are found [Feldstein and Starkov, 1967; Meng, 1977; Gussenhoven et al., 1981 and 1983; see also Chapter 12]. The optical emissions are a result of the energy from precipitating energetic particles (mostly electrons) being deposited in the ionosphere. Optical emissions visible to the naked eye are mostly in narrow latitudinal bands (1 to 10 km in width) called auroral arcs, but there are precipitating particles and optical emissions throughout the auroral zone. In the equatorward portion of the auroral oval the optical emissions are spatially uniform and are known as the diffuse aurora. Along the poleward portion of the oval, the precipitating particles tend to be grouped into bands about 1° wide. The intensity and maximum energy of the precipitating particles are greatest in the center of the band and fall off near the edges of the band. These have been called "inverted-V" events due to their signature in the records of polar orbiting satellites. If the maximum intensity is great enough, a visible auroral arc will appear at the center of the inverted-V event.

The precipitating energetic particles lose energy to the atmosphere by ionizing neutrals in a manner similar to the ionization caused by protons. If the precipitating particles all had the same energy, a thin layer of ionization would be formed. The altitude of the ionization layer is determined from the energy of the precipitating particles: 10 keV electrons produce an ionization layer near 110 km altitude; 500 eV electrons produce an ionization layer near 180 km altitude. The density of the ionization layer is determined by the intensity of the particle flux.

In the nighttime auroral zone, the electron density profile can be accurately estimated if the spectrum of precipitating particles is known, or conversely the spectrum of precipitating particles can be estimated from the electron density profile [Vondrak and Baron, 1977]. This is especially true in the E region where the ionization lifetimes are short. In the F region where ionization lifetimes are long, the ionization present at any given moment is influenced by the precipitation over the past few minutes to tens of minutes as well as the instantaneous precipitation. Also, vertical and horizontal transport has a major effect upon the structure of the F region. Regions of enhanced F region ionization can drift many degrees from the production region [Vickrey et al., 1980].

In the sunlit auroral zone, photoionization dominates the production of ionization, but ionization from particles has a major effect on plasma irregularities. Also, in limited altitude regions the ionization from particles can occasionally dominate photoionization. Even where the photoionization is the dominant source, the heat from precipitating particles increases the scale height of the ionosphere and the neutrals.

An important feature of the high latitude ionosphere is that the plasma density is irregular on the scale of meters to kilometers vertically and on the scale of meters to hundred of kilometers horizontally. The small scale irregularities cause scintillation of radio signals passing through the ionosphere. The large scale irregularities or density gradients provide a necessary condition for various plasma turbulence mechanisms that result in small scale irregularities (see Chapter 10). The causes of irregularities in the auroral zone are numerous [Fejer and Kelley, 1980] but are related to factors such as particle precipitation and E × B drifts. The region of auroral zone scintillations extends equatorward of the optical auroral [Martin and Aarons, 1977], but are roughly collocated with the region of particle precipitation. Some of the strongest scintillations are observed when the ray path of the radio signal is aligned with the magnetic L-shell in the F region. This has been analyzed to indicate that irregularities are in the form of sheets extended along the magnetic field and in the magnetic E-W direction [Rino et al., 1978].

9.2.3 Substorm Effects.

In the ionosphere, a substorm is an intensification of processes and structures that are normally observed in the quiet time auroral zone ionosphere. See Chapter 8 for a complete description. During a substorm the flux and average energy of the precipitating particles increase rapidly and substantially. This causes more visible features to appear. The increase in the energy of the particle causes ionization in the lower E layer that is not present during quiet times. The increased activity causes an increase in the scintillation producing irregularities. The increased E × B drift rates heat the ionosphere and increase the scale heights.

During the early phases of a substorm, the auroral zone moves equatorward several degrees in 10–20 minutes. The trough either moves equatorward with the auroral zone movement or ceases to exist during the substorm depending on geomagnetic conditions and local time. During the late phases of a substorm the auroral oval contracts poleward and precipitation induced ionization tends to die away by recombination.

9.2.4 Polar Cap Structure.

The polar cap ionosphere is relatively placid compared to the auroral zone, but soft particle precipitation known as polar rain [Winningham and Heikkila, 1974] does affect the polar cap ionosphere. In the summer months, the polar cap ionosphere is dominated by photoionization similar to the midlatitude ionosphere. In the winter months, ionization is generally maintained by the polar rain and by convection from the day side to the night side of the polar cap. In the winter months, the F layer can be sunlit while the E layer is in darkness. This can lead to He^+ being the dominant

ion in parts of the topside ionosphere. During times of weak convection and precipitation, the winter polar ionosphere near the midnight sector can decay to very low levels of ionization; this area is called the polar hole [Brinton et al., 1978].

Since the magnetic field lines in the polar cap diverge effectively toward infinity, the H^+ in the polar ionosphere escapes rapidly in a process known as the polar wind. Unlike the midlatitude ionosphere, O^+ is generally the dominant ion at all altitudes of the F-region.

9.3 EQUATORIAL PHENOMENA

9.3.1 Sq Current System

See Chapter 4.

9.3.2 Equatorial Electrojet

The intense eastward ionospheric current that flows by day over a narrow latitudinal strip along the magnetic equator is known as the *equatorial electrojet* [Matsushita and Campbell, 1967]. The electrojet causes the large daily variations of the horizontal component of magnetic field intensity recorded by ground magnetometers near the magnetic equator. The ionospheric current system is a result of a dynamo action of the horizontal wind system and the electrical conductivity of the ionosphere in the presence of the electrons and ions. The concentration of ionospheric current near the magnetic equator is a result of the high value of electrical conductivity of the upper atmosphere at the dip equator, which arises from an inhibition of Hall current due to the horizontal configuration of the earth's magnetic field and the horizontal stratification of the ionosphere.

The electrical conductivity of the ionosphere is not only governed by the concentration of the charged particles but by the neutral particles and the earth's magnetic field as well [Chapman, 1956]. Through collisions the neutral particles restrict the motion of charged particles under the action of any impressed electric field. The presence of the magnetic field, on the other hand, restricts the motion of charged particles across the magnetic field and therefore makes the conductivity anisotropic.

When a dc electric field is impressed parallel to the magnetic field, the longitudinal electrical conductivity that exists parallel to the magnetic field is given by

$$\sigma_o = ne^2 \left[\frac{1}{m_e \nu_e} + \frac{1}{m_i \nu_i} \right], \qquad (9.8)$$

where n is the electron or ion concentration, e is the electronic charge, ν_e and ν_i are the electron and ion collision frequencies, and m_e and m_i are the masses of an electron and an ion respectively. The longitudinal conductivity is independent of magnetic field intensity and is identical to the conductivity obtained in the absence of any magnetic field.

When an electric field is applied perpendicular to the magnetic field, the conductivity in the direction of the electric field is called the Pedersen conductivity and is given by

$$\sigma_1 = ne^2 \left[\frac{\nu_e}{m_e\left(\nu_e^2 + \Omega_e^2\right)} + \frac{\nu_i}{m_i\left(\nu_i^2 + \Omega_i^2\right)} \right], \qquad (9.9)$$

where Ω_e and Ω_i are the electron and ion gyrofrequencies respectively.

In such cases of a crossed electric and magnetic field, a Hall current usually flows perpendicular to both the electric and magnetic fields and the resulting conductivity, called the Hall conductivity, is given by

$$\sigma_2 = ne^2 \left[-\frac{\Omega_e}{m_e\left(\nu_e^2 + \Omega_e^2\right)} + \frac{\Omega_i}{m_i\left(\nu_i^2 + \Omega_i^2\right)} \right]. \qquad (9.10)$$

At the magnetic equator, an eastward electric field is developed by the dynamo action of the horizontal wind system, which gives rise to a motion of charged particles in the east-west direction (X) due to the Pedersen conductivity σ_1 and in the vertical direction (Z) due to the Hall conductivity σ_2. In view of the horizontal stratification of the ionosphere, the flow of Hall current in the vertical direction (Z) is totally inhibited and a polarization electric field (E_Z) develops. In such a case the current densities J_X, J_Z in the X and Z directions can be expressed as

$$J_X = \sigma_1 E_X + \sigma_2 E_Z$$

$$J_Z = -\sigma_2 E_X + \sigma_1 E_Z = 0$$

or,
$$J_X = \left(\sigma_1 + \frac{\sigma_2^2}{\sigma_1}\right) E_X$$

or,
$$J_X/E_X = \sigma_1 + \frac{\sigma_2^2}{\sigma_1}$$

$$= \sigma_3 . \qquad (9.11)$$

The resulting conductivity in the east-west direction is called the Cowling conductivity σ_3.

The variations of Pederson σ_1, Hall σ_2, and Cowling σ_3 conductivities with altitude at the magnetic equator are

shown in Figure 9-3a for an assumed variation of electron density N and temperature T shown in Figure 9-3b. The enhanced value of the Cowling conductivity in the dynamo region is sufficient to account for the intensity of the equatorial electrojet. Away from the equator, the geomagnetic

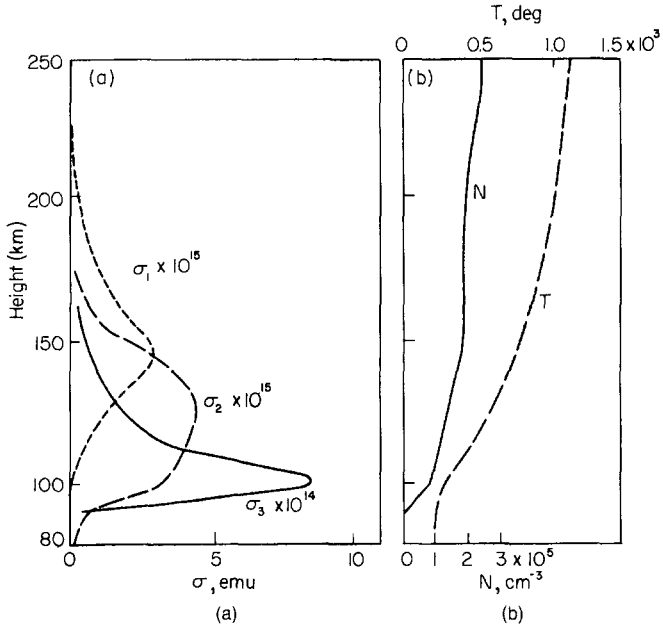

Figure 9-3. (a) Variation of Pedersen σ_1, Hall σ_2, and Cowling σ_3 conductivities with altitude for an ionosphere in which electron density N and temperature T vary as shown at (b). Note that scale for σ_3 is smaller than σ_1 and σ_2 by a factor of 10 [Chapman and Raja Rao, 1965, based on Chapman, 1956].

field is no longer horizontal, which allows the Hall field to leak away. Baker and Martyn [1952] estimated that the half-width of the strip of enhanced east-west conductivity around the dip equator is about 3° in latitude. The equatorial electrojet corresponds to an east-west electric field of 0.5 mV/m and a vertical polarization field of about 10 mV/m. This gives rise to an eastward current or westward electron drift of several hundred m/s. The electron drift is westward by day and eastward at night. This electrojet model was studied in detail by Sugiura and Cain [1966]. More complete models allowing for vertical currents have been discussed by Untiedt [1967], Sugiura and Poros [1969], Richmond [1973], and others.

The equatorial electrojet current has been observed to reverse its normal direction during day or night and during magnetically quiet or disturbed condtions; this reverse current system has been termed the *counter electrojet* [Gouin and Mayaud, 1967; Hutton and Oyinloye, 1970; Rastogi, 1973; Fejer et al., 1976; Fejer and Kelley, 1980]. The rapid reversals during disturbed conditions have been related to magnetospheric and high-latitude phenomena [Matsushita and Balsley, 1972], whereas the reversals during quiet conditions have been related to lunar tides [Rastogi, 1974].

9.3.3 Electrojet Irregularities

Ionosondes first detected the existence of a distinct type of sporadic E near the magnetic equator which is patchy and transparent to radio waves reflected from higher layers. The intensity of equatorial E_s (or E_{sq}) is strongly correlated with the strength of the electrojet current discussed in the last section [Matsushita, 1951]. A typical ionogram showing E_{sq} echoes is shown in Figure 9-4. VHF forward scatter

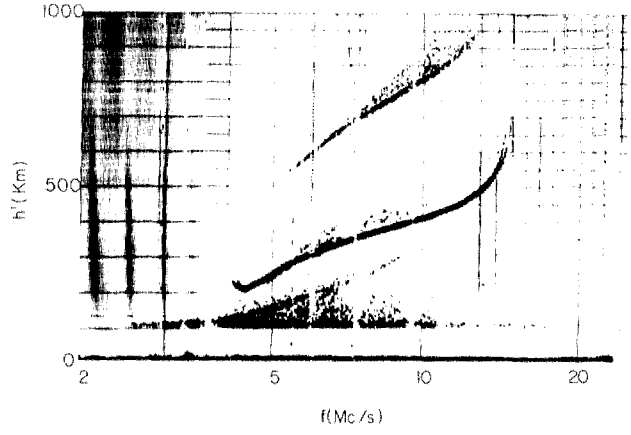

Figure 9-4. The typical equatorial sporadic E configuration on an ionogram recorded at Huancayo, Peru at 1229 hr (75°W) on 19 April 1960 [Cohen et al., 1962].

experiments established that these echoes arise as a result of scattering from field aligned irregularities of electron density immersed in the equatorial electroject [Bowles and Cohen, 1962].

The important characteristics of the electrojet irregularities as related to the physics of the scattering region have been probed by the VHF radar measurements performed at the Jicamarca Radio Observatory. Radar spectral studies have shown the existence of two classes of irregularities called Type 1 and Type 2, associated with the electrojet [Balsley and Farley, 1973; Farley and Balsley, 1973; Fejer and Kelley, 1980].

Type 1 irregularities have a very narrow spectrum with a Doppler shift corresponding approximately to the ion acoustic velocity of about 360 m/s. Farley [1963] and Buneman [1963] have explained the Type 1 irregularities by showing that a plasma is unstable to waves when the relative electron-ion drift velocity in the direction of the wave exceeds the ion acoustic velocity. As such, Type 1 irregularities are also called two-stream irregularities. Type 2 irregularities on the other hand have phase velocities smaller than the ion-acoustic velocity and are observed even when the eastward drift velocity is very small during the day. Type 2 irregularities are identified with E_{sq} echoes in ionograms and both disappear under counter electrojet condi-

tions during the daytime. At night the Type 2 irregularities are almost always observed except for momentary disappearance when the electrojet electric field reverses sign. The Type 2 irregularities are explained by the gradient drift instability mechanism. This is because the horizontal polarization field arising from a relative electron-ion drift in the electrojet region can, in the presence of the earth's magnetic field, develop a drift in the direction of the vertically oriented density gradient and give rise to these irregularities [Fejer and Kelley, 1980].

9.3.4 Equatorial Anomaly and Fountain Effect

During the equinox the sun is overhead at the equator, and in terms of solar control the ionization density is expected to be maximum in that region. Instead, the daytime ionization density at the F_2 peak shows a pronounced trough at the magnetic equator and crests at about 30°N and 30°S magnetic dip. This anomalous latitude variation of F_2 ionization near the magnetic equator obtained from bottomside ionograms illustrated in Figure 9-5, was first recognized by

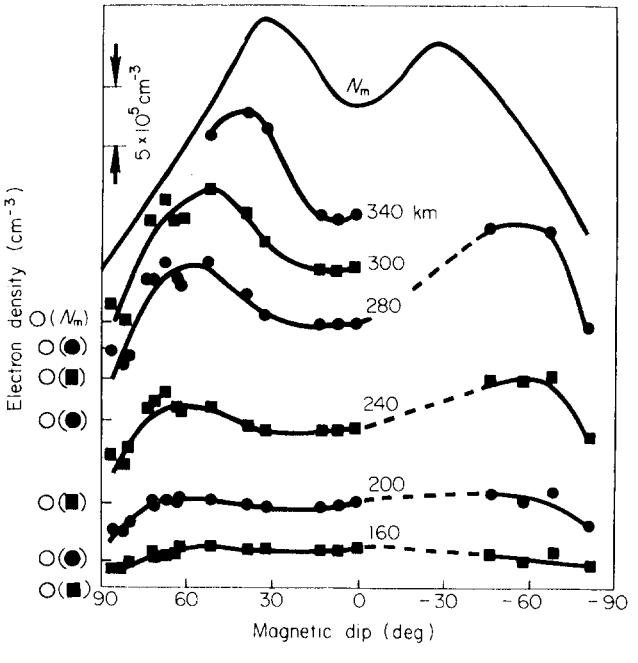

Figure 9-5. Variation of N_mF_2 and of electron density (electron concentration) at fixed heights with magnetic dip, for noon on magnetically quiet days in September 1957. The zero level for each curve is indicated on the left [Croom et al., 1959]. Reprinted with permission from MacMillan Journals Ltd., © 1959.)

Appleton [1946] and is known as the equatorial anomaly or *Appleton* anomaly.

The equatorial anomaly is explained in terms of a *fountain effect* caused by vertical electrodynamic drift at the equator and plasma diffusion along geomagnetic field lines [Martyn, 1959]. Figure 9-6 illustrates how the eastward E-region dynamo electric field at locations slightly off the magnetic equator maps to F-region altitude over the equator. The eastward electric field in conjunction with the northward

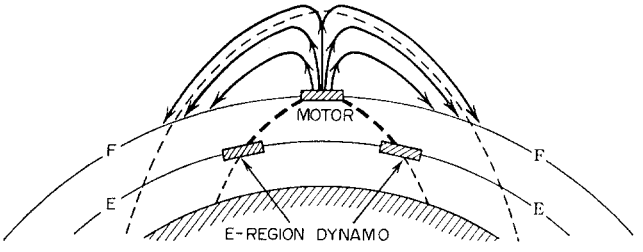

Figure 9-6. The F region geomagnetic anomaly. Near the equator the electric fields of the atmospheric dynamo in the E layer are conveyed upwards along geomagnetic lines of force to the *motor* in the F layer where they produce an upwards movement of the plasma during the day. The raised plasma then diffuses down lines of force to produce enhanced concentration at places on each side of the equator and decreased concentration at the equator itself [Ratcliffe, 1972].

geomagnetic field gives rise to a vertically upward plasma motion. At high altitudes over the equator, the plasma encounters field lines that connect to the F_2 peak at 30°N and 30°S magnetic dip along which the plasma diffuses under the action of gravity. Such plasma transport depletes the F_2 ionization at the equator and increases the density at locations 30°N and 30°S. Theoretical studies of the equatorial anomaly on a more rigorous basis have been performed by many workers [see Hanson and Moffett, 1966 and references therein].

The transport processes involved in the formation of the equatorial anomaly are best illustrated by the Alouette I topside sounder results. Figure 9-7 shows the variation of ionization density as a function of height and latitude in the daytime topside ionosphere. At high altitudes over the magnetic equator, the density shows a dome-like structure following the shape of a magnetic field line. At lower altitudes, below 700 km, a field-aligned double humped structure is obtained, with the maxima being closer together at the greater heights.

The diurnal development of the equatorial anomaly has been studied from ground based as well as topside sounders. Ground based data indicate that during years of sunspot minimum the anomaly is most pronounced at about 1400 LT and then declines steadily until it disappears around 2000 LT [Rastogi, 1959]. However, during the period of sunspot maximum, the anomaly after an initial decay in the afternoon hours shows substantial redevelopment in the late evening hours [Martyn, 1959; Appleton, 1960; Wright, 1960] and often the ionization density at the crests in the evening period exceeds the daytime values. Latitudinal asymmetry of the equatorial anomaly in the northern and southern hemisphere as a function of season and longitude has also been studied

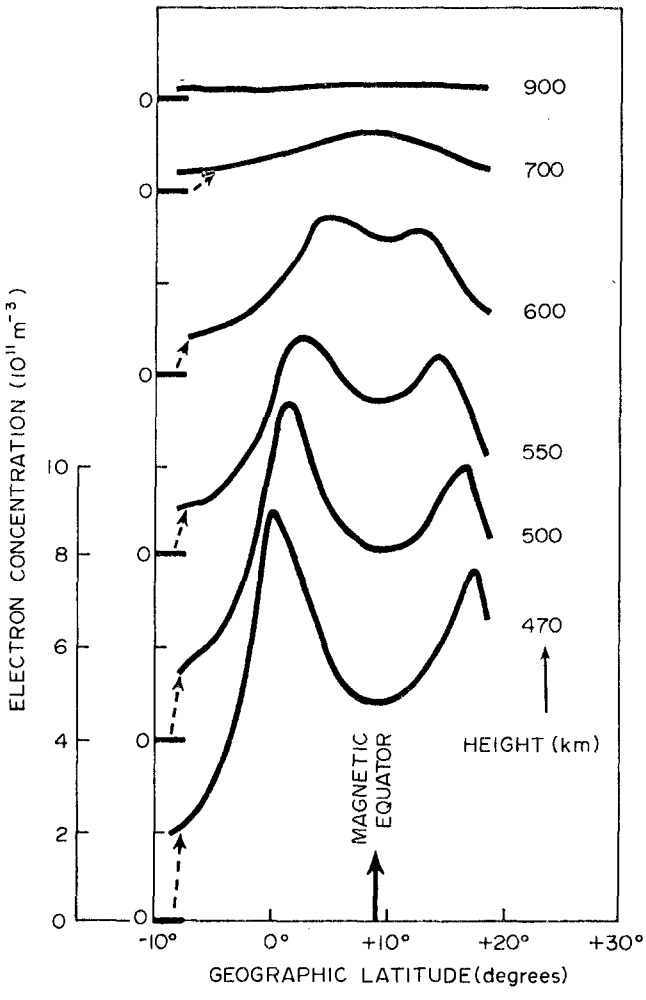

Figure 9-7. Latitudinal variation of electron density across the equatorial anomaly at various altitudes above h_{max} from topside ionograms [Eccles and King, 1969]. (Reprinted with permission from IEEE © 1969.)

[Lyon, 1963; Lyon and Thomas, 1963]. Interhemispheric neutral wind and variation of magnetic declination with longitude have been invoked in theoretical models [Hanson and Moffett, 1966] to account for such asymmetry.

9.3.5 Equatorial F Region Irregularities

Historically, the signature of equatorial nighttime F-region irregularities was first obtained from the spread-F signature on ionograms [Booker and Wells, 1938]. Equatorial spread-F has since been divided into two types, range and frequency spread [Calvert and Cohen, 1961; Rastogi, 1980], the former type being attributed to strongly scattering irregularities.

The advent of orbiting and geostationary beacons in the early 1960s provided another technique for monitoring equatorial irregularities, that of measuring the phase, amplitude, and plane of polarization of the trans-ionospherically propagated signal. The bulk of the information on magnitude and occurrence of these irregularities came from amplitude fluctuation or scintillation measurements at a host of equatorial stations (see Chapter 10 for further details).

During the last decade a determined effort has been made to understand the nature and occurrence of nighttime equatorial F-region irregularities since the largest propagation effects extending up to S-band frequencies are observed in this region. Our insight has come from multi-technique observations comprising satellite and rocket *in situ* measurement of irregularity amplitude and spectra, coherent and incoherent radar backscatter measurements, total electron content and ground based and airborne multi-frequency scintillation, and all-sky imaging photometer measurements. Together these techniques measure irregularities over scale lengths of 5 to 6 orders of magnitude from hundreds of kilometers to tens of centimeters, and given the right conditions the post-sunset equatorial F-region is indeed found to contain irregularities over this enormous scale size range [Basu and Basu, 1981]. A brief description of the different techniques and their results are given below.

The rocket and satellite *in situ* measurements have detected large scale irregular biteouts of ion concentration (N_i) in the nighttime equatorial spread-F region associated with small scale irregularities in N_i [Hanson and Sanatani, 1973; Kelley et al., 1976; Morse et al., 1977]. A comprehensive study of such depleted regions by McClure et al., [1977] indicates the presence of very sharp electron density structures (see bottom panel of Figure 9-8) and the existence of ionic species near the F-peak that are normally obtained in the bottomside and valley region between the E and F layers. This study also revealed the existence of a highly structured upward velocity within these depleted regions on the order of 100 m/s (hence the name *bubbles*), and sometimes, in addition, a westward velocity of about 20 m/s as shown in

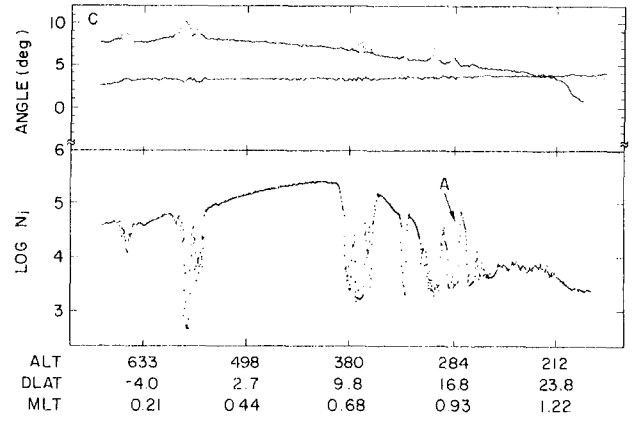

Figure 9-8. Ion drift meter data, orbit 2282. Satellite altitude, dip latitude, and magnetic local time are indicated on the figure. The satellite longitude was $-50°$ to $-65°$. The observed pitch and yaw angles are shown in the upper and lower curves, respecitively. Positive angles correspond to ions moving up or left with respect to the spacecraft [McClure et al., 1977].

Figure 9-8. Woodman and LaHoz [1976] using the radar technique at Jicamarca observed plume-like structures in backscatter power maps of equatorial irregularities at 3 m wave length. The maps they obtained are similar to that shown in the top panel of Figure 9-9. They interpret the plumes as being due to vertically rising bubbles and their wakes. Evidence for the fact that the plasma bubbles, most probably initiated by the Rayleigh-Taylor instability, are probably extended in altitude has been obtained from conventional polarimeter observations of the total electron content (TEC). These observations [Yeh et al., 1979; DasGupta et al., 1982] show that scintillation patches in the early evening hours occur in association with depletions of TEC which may be as large as 40% of the ambient value.

From topside sounder observations, Dyson and Benson [1978] have shown that plasma bubbles are confined within magnetic field tubes. By the use of an all sky imaging photometer on board an aircraft, Weber et al., [1978, 1980] have detected 6300 Å airglow depletions in the nighttime equatorial F-region in association with radar backscatter and scintillation patches. The 6300 Å airglow depletions signify depletions of integrated ionization density and the two-dimensional maps of these structures show that the depletions observed near the magnetic equator have typical E-W dimension of 100 km and are as large as 1200 km in the magnetic N-S direction. These observations establish that the bubbles are open at the bottom and confined within magnetic field tubes. From measurements of both incoherent scatter and coherent backscatter using a steerable radar at 155 MHz, Tsunoda [1980a] located the 1 m field aligned irregularities at the top edge of a plasma bubble and mapped the bubble along the magnetic field tube.

By performing careful coordinated studies of radar backscatter, high resolution satellite and rocket *in situ* and ground scintillation measurements, the spatial and temporal coexistence of kilometer and meter scale irregularities have been studied [Basu et al., 1978; 1980; Rino et al., 1981]. Figure 9-9, taken from Basu and Basu [1981], shows that the 3 m irregularities causing the radar backscatter and kilometer to several hundred meter irregularities causing scintillations are simultaneously (within the limit of time resolution of the experiment ~ min) generated in the onset phase, but the short scale irregularities are outlived by the large scale ones by several hours. A considerable effort has been made

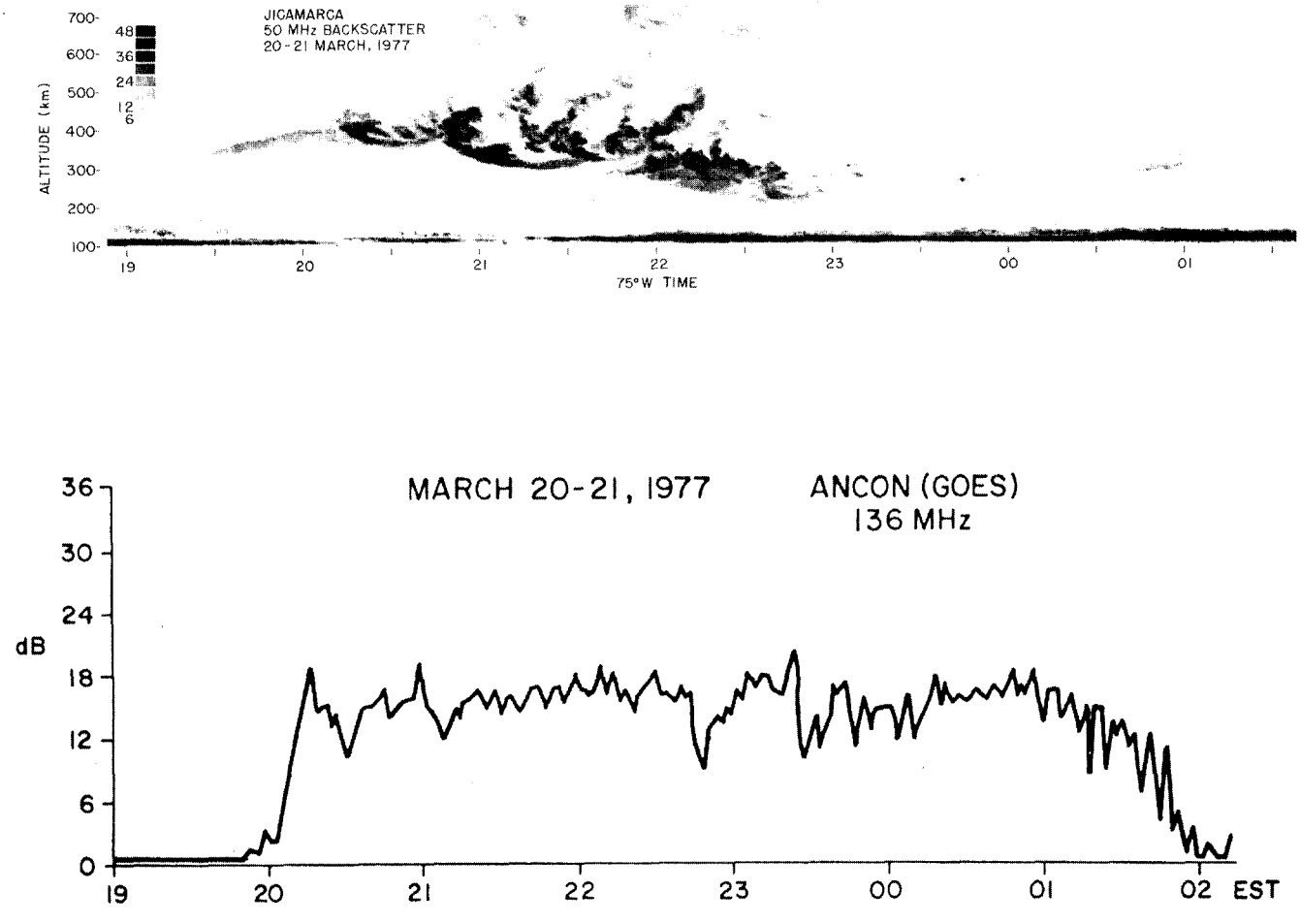

Figure 9-9. Temporal variation of range and intensity (different grey tones) of 50 MHz backscattered power at Jicamarca on 20–21 March 1977 (top panel) and 137 MHz scintillations (bottom panel) over a nearly common ionospheric volume [Basu et al., 1980].

over the past few years to detect irregularities shorter than the ion gyroradius which is ~5 m in the topside equatorial ionosphere [Woodman and Basu, 1978] for radar system applications and for the understanding of the complex plasma processes in equatorial spread F. By the use of the ALTAIR radar at Kwajalein, Marshall Islands, irregularities with spatial wavelengths of 1 m and 36 cm have been detected [Tsunoda et al., 1979; Towle, 1980; Tsunoda, 1980b] and more recently the TRADEX radar at Kwajalein has been used to detect 11 cm irregularities which are approximately 3 times the electron gyroradius and 30 times the Debye length [Tsunoda, 1980c]. Thus equatorial spread F is found to encompass irregularity wavelengths extending over 5–6 orders of magnitude.

CHAPTER 9

REFERENCES

Ahmed, M., R.C. Sagalyn, and P.J.L. Wildman, "Topside Ionosphere Trough Morphology: Occurrence Frequency and Diurnal, Seasonal and Altitude Variations," *J. Geophys. Res.*, **84:** 489–498, 1979.

Appleton, E.V., "Two Anomalies in the Ionosphere," *Nature* (London), **157:** 691, 1946.

Appleton, E.V., "Two Anomalies in the Behavior of the F2 Layer of the Ionosphere," *Some Ionospheric Results Obtained During the IGY.*, edited by W.J.G. Beynon, p. 3, Elsevier, Amsterdam, 1960.

Baker, W.G. and D.F. Martyn, "Conductivity of the Ionosphere," *Nature*, **170:** 1090, 1952.

Balsley, B.B. and D.T. Farley, "Radar Observations of Two-Dimensional Turbulence in the Equatorial Electrojet," *J. Geophys. Res.*, **78:** 7174, 1973.

Banks, P.M. and G. Kockarts, *Aeronomy, Part B*, Academic Press, New York, 1973.

Basu, S. and Su. Basu, "Equatorial Scintillations—A Review," *J. Atmos. Terr. Phys.*, **43:** 473, 1981.

Basu, S., Su. Basu, J. Aarons, J.P. McClure, and M.D. Cousins, "On the Coexistence of Kilometer- and Meter-Scale Irregularities in the Nighttime Equatorial F Region," *J. Geophys. Res.*, **83:** 4219, 1978.

Basu, S., J.P. McClure, S. Basu, W.B. Hanson, and J. Aarons, "Coordinated Study of Equatorial Scintillation and In Situ and Radar Observations of Nighttime F Region Irregularities," *J. Geophys. Res.*, **85:** 5119, 1980.

Booker, H.G. and H.W. Wells, "Scattering of Radio Waves by the F-Region of the Ionosphere," *Terr. Magn. Atmos. Elect.*, **43:** 249, 1938.

Bowles, K.L. and R. Cohen, "A Study of Radio Wave Scattering from Sporadic E. Near the Magnetic Equator," in *Ionospheric Sporadic E*, edited by E.K. Smith and S. Matsushita, Pergamon Press, New York, 1962.

Brinton, H.C., J.M. Grebowsky, and L.H. Brace, "The High Latitude Winter F-Region at 300 km: Thermal Plasmas Observations from AE-C," *J. Geophys. Res.*, **83:** 4767–4776, 1978.

Buneman, O., "Excitation of Field Aligned Sound Waves by Electron Streams," *Phys. Res. Lett.*, **10:** 285, 1963.

Calvert, W. and R. Cohen, "The Interpretation and Synthesis of Certain Spread-F Configurations Appearing on Equatorial Ionograms," *J. Geophys. Res.*, **66:** 3125, 1961.

Carpenter, D.L. and C.G. Park, "On What Ionospheric Workers Should Know About the Plasmapause-Plasmasphere," *Rev. Geophys. Space Sci.*, **11:** 133–154, 1973.

Chapman, S., "The Electrical Conductivity of the Ionosphere: A Review," *Nuovo Cimento*, **4**(Suppl): 1385, 1956.

Chapman, S. and K.S. Raja Rao, "The H and Z Variations Along and Near the Equatorial Electrojet in India, Africa and the Pacific," *J. Atmos. Terr. Phys.*, **27:** 559–581, 1965.

Cohen, R., K.L. Bowles, and W. Calvert, "On the Nature of Equatorial Slant Sporadic E," *J. Geophys. Res.* **67:** 965–972, 1962.

Cormier, R.J., "Thule Riometer Observations of Polar Cap Absorption Events, (1962–1972)," AFCRL TR-73-0060, 1973.

Croom, S., A. Robbins, and J.O. Thomas, "A Review of Topside Sounder Studies of the Equatorial Ionosphere," *Nature* (London), **184:** 2003, 1959.

DasGupta, A., J. Aarons, J.A. Klobuchar, S. Basu, and I. Bushby, "Ionsopheric Electron Content Depletions Associated with Amplitude Scintillations in the Equatorial Region," *Geophys. Res. Lett.*, **9:** 147–150, 1982.

DNA Ratebook, Defense Nuclear Agency, U.S. Government Printing Office, Washington, D.C., 1972.

Doering, J.P., T.A. Potemra, W.K. Petersen, and C.O. Bostrom, "Characteristic Energy Spectra of 1 to 500 eV Electrons Observed in the High Latitude Ionosphere from Atmospheric Explorer C," *J. Geophys. Res.*, **81:** 5507, 1976.

Donnelly, R.F., "Contribution of X-Ray and EUV Bursts of Solar Flares to Sudden Frequency Deviations," *J. Geophys. Res.*, **74:** 1973, 1969.

Donnelly, R.F., "Extreme Ultraviolet Flashes of Solar Flares Observed Via Sudden Frequency Deviations: Experimental Results," *Sol. Phys.*, **29:** 188, 1971.

Dyson, P.L. and R.F. Benson, "Topside Sounder Observations of Equatorial Bubbles," *Geophys. Res. Lett.*, **5:** 795, 1978.

Eccles, D. and J.W. King, "A Review of Topside Sounder Studies of the Equatorial Ionosphere," *Proc. IEEE*, **57:** 1012, 1969.

Evans, J.V., "Incoherent Scatter Contributions to Studies of the Dynamics of the Lower Thermosphere," *Rev. Geophys. Space Sci.*, **16:** 195–216, 1978.

Farley, D.T., "A Plasma Instability Resulting in Field-Aligned Irregularities in the Ionosphere," *J. Geophys. Res.*, **68:** 6083, 1963.

Farley, D.T. and B.B. Balsley, "Instabilities in the Equatorial Electrojet," *J. Geophys. Res.*, **78:** 227, 1973.

Fejer, B., D.T. Farley, B.B. Balsley, and R.F. Woodman, "Radar Studies of Anomalous Velocity Reversals in the Equatorial Ionosphere," *J. Geophys. Res.*, **81:** 4621, 1976.

Fejer, B.G. and M.C. Kelley, "Ionospheric Irregularities," *Rev. Geophys. Space Sci.*, **18:** 401–454, 1980.

Feldstein, Y.I. and G.V. Starkov, "Dynamics of Auroral Belts and Polar Geomagnetic Disturbances," *Planet. Space Sci.*, **15:** 209, 1967.

Ferguson, E.E., "D-Region Ion Chemistry," *Rev. Geophys. Space Phys.*, **9:** 997–1008, 1971.

Gouin, P. and P.N. Mayaud, "A Propos de Existence Possible d'un Contre-electrojet aux Latitudes Magnetiques Equatoriales," *Ann. Geophys.*, **23:** 41, 1967.

Gussenhoven, M.S., D.A. Hardy, and W.J. Burke, "DMSP/F2 Electron Observations of Equatorward Auroral Boundaries and Their Relationship to Magnetospheric Electric Fields," *J. Geophys. Res.*, **86:** 768, 1981.

Gussenhoven, M.S., D.A. Hardy, N. Heinemann, and E. Holeman, "1978 Diffuse Auroral Boundaries and a De-

rived Auroral Boundary Index," AFGL TR-82-0398, ADA130175, 1982.

Hanson, W.B. and R.J. Moffett, "Ionization Transport Effects in the Equatorial F Region," *J. Geophys. Res.*, **71:** 5559, 1966.

Hanson, W.B. and S. Sanatani, "Large N_i Gradients Below the Equatorial F- Peak," *J. Geophys. Res.*, **78:** 1167, 1973.

Hudson, R.D., "Critical Review of Ultraviolet Photoabsorption Cross Section for Molecules of Astrophysical and Aeronomic Interest," *Rev. Geophys. Space Phys.*, **9:** 305–406, 1971.

Hutton, R. and J.O. Oyinloye, "The Counter-Electrojet in Nigeria," *Ann. Geophys.*, **26:** 921, 1970.

Jasperse, J.R., "Electron Distribution Function and Ion Concentrations in the Earth's Lower Ionosphere from Boltzman-Fokker-Planck Theory," *Planet. Space Sci.*, **25:** 743, 1977.

Kelley, M.C., G. Haerendel, H. Kappler, A. Valenzuela, B.B. Balsley, D.A. Carter, W.L. Eklund, C.W. Carlson, B. Hausler, and R. Torbert, "Evidence for a Rayleigh-Taylor Type Instability and Upwelling of Depleted Density Regions during Equatorial Spread-F," *Geophys. Res. Lett.*, **3:** 448, 1976.

Kohnlein, W., "Electron Density Models of the Ionosphere," *Rev. of Geophys. Space Phys.*, **16:** 341–354, 1978.

Lyon, A.J., *The Ionosphere*, p. 88, Physical Society, London, 1963.

Lyon, A.J. and L. Thomas, "The F2-Region Equatorial Anomaly in the African, American and East Asian Sectors during Sunspot Maximum," *J. Atmos. Terr. Phys.*, **25:** 373, 1963.

Mantas, G.P., H.C. Carlson, and V.B. Wickwar, "Photoelectron Flux Build-up in the Plasmasphere," *J. Geophys. Res.*, **83:** 1–15, 1978.

Martin, E. and J. Aarons, "F-Layer Scintillations and Aurora," *J. Geophys. Res.*, **82:** 2717–2722, 1977.

Martyn, D.F., *The Physics of the Ionosphere*, p. 254, Physical Society, London, 1963.

Martyn, D.F., "The Normal F Region of the Ionosphere," *Proc. IRE N.Y.*, **47:** 147, 1959.

Matsushita, S., "Intense E_s Ionization Near the Magnetic Equator," *J. Geomagn. Geoelect.*, **3:** 44–46.

Matsushita, S. and B.B. Balsley, "A Question of DP-2," *Planet. Space Sci.*, **20:** 1259, 1972.

Matsushita, S. and W.H. Campbell (eds.), *Physics of Geomagnetic Phenomena*, Academic Press, New York, 1967.

McClure, J.P., W.B. Hanson, and J.H. Hoffman, "Plasma Bubbles and Irregularities in the Equatorial Ionosphere," *J. Geophys. Res.*, **82:** 2650, 1977.

Meng, C.-I., R.H. Holzworth, and W.-I. Akasofu, "Auroral Circle Delineating the Poleward Boundary of the Quiet Auroral Oval," *J. Geophys. Res.*, **82:** 164, 1977.

Morse, F.A., B.C. Edgar, H.C. Koons, C.J. Rice, W.J. Heikkila, J.H. Hoffman, B.A. Timsley, J.D. Winningham, A.B. Christiansen, R.F. Woodman, J. Pomalaza, and R.N. Teixeiro, "Equion: An Equatorial Ionospheric Irregularity Experiment," *J. Geophys. Res.*, **82:** 578, 1977.

Rasmussen, J.E., P.A. Kossey, and E.A. Lewis, "Evidence of an Ionospheric Reflecting Layer Below the Classical D Region," *J. Geophys. Res.*, **85:** 3037–3044, 1980.

Rastogi, R.G., "The Diurnal Development of the Anomalous Equatorial Belt in the F2 Region of the Ionosphere," *J. Geophys. Res.*, **64:** 727, 1959.

Rastogi, R.G., "Counter Electrojet Currents in the Indian Zone," *Planet. Space Sci.*, **21:** 1355, 1973.

Rastogi, R.G., "Lunar Effects in the Counter-Electrojet Near the Magnetic Equator," *J. Atmos. Terr. Phys.*, **36:** 167, 1974.

Rastogi, R.G., "Seasonal and Solar Cycle Variations of Equatorial Spread-F in the American Zone," *J. Atmos. Terr. Phys.*, **42:** 593, 1980.

Ratcliffe, J.A., *An Introduction to the Ionosphere and Magnetosphere*, Cambridge University Press, 1972.

Richmond, A.D., "Equatorial Electrojet, I. Development of a Model Including Winds and Instabilities," *J. Atmos. Terr. Phys.*, **35:** 1083, 1973.

Richmond, A.D., and S.V. Venkateswaran, "Geomagnetic Crochets and Associated Ionospheric Current Systems," *Radio Sci.*, **6:** 139, 1971.

Rino, C.L., T. Tsunoda, J. Petriceks, R.C. Livingston, M.C. Kelley, and K.D. Baker, "Simultaneous Rocket-Borne Beacon and in situ Measurements of Equatorial Spread-F—Intermediate Wavelength Results," *J. Geophys. Res.*, **86:** 2411, 1981.

Rino, C.L., R.C. Livingston, and S.J. Matthews, "Evidence for Sheet-Like Auroral Ionospheric Irregularities," *Geophys. Res. Lett.*, **5:** 1039, 1978.

Roble, R.G., R.E. Dickinson, E.C. Ridley, and Y. Kamide, "Thermospheric Response to the November 8–9, 1969 Disturbance," *J. Geophys. Res.*, **84:** 4207–4216, 1979; "Thermosphere Circulation Models," *Eos, Trans. AGU*, **62:** 3, 19, 1981.

Sojka, J.J., W.J. Raitt, and R.W. Schunk, "A Theoretical Study of High Latitude Winter F Region at Solar Minimum for Low Magnetic Activity," *J. Geophys. Res.*, **86:** 609–621, 1981.

Stolarski, R.S. and N.P. Johnson, "Photoionization and Photoabsorption Cross Sections for Ionospheric Calculations," *J. Atmos. Terr. Phys.*, **34:** 1691, 1972.

Strascio, M.A. and B. Sellers, "The Calculation of Riometers Absorption and Approximate Connection Between Riometer Absorptions and Solar Proton Fluxes during Night-Time PCA Events," AFCRL TR-75-0469, ADA019656, 1975.

Sugiura, M. and J.C. Cain, "A Model Equatorial Electrojet," *J. Geophys. Res.*, **71:** 1869, 1966.

Sugiura, M. and D.J. Poros, "An Improved Model Equatorial Electrojet with a Meridional Current System," *J. Geophys. Res.*, **74:** 4025, 1969.

Titheridge, J.E., "Ion Transition Heights from Topside Electron Density Profiles," *Planet. Space Sci.*, **24:** 229–245, 1976.

Torr, D.G., "Ionospheric Chemistry," *Rev. Geophys. Space Phys.*, **17:** 510–521, 1979.

Towle, D.M., "VHF and UHF Radar Observations of Equatorial Ionospheric Irregularities and Background Densities," *Radio Sci.*, **15:** 71, 1980.

Tsunoda, R.T., "Magnetic-Field-Aligned Characteristics of Plasma Bubbles in the Nighttime Equatorial Ionosphere," *J. Atmos. Terr. Phys.*, **42:** 743, 1980a.

Tsunoda, R.T., "On the Spatial Relationship of 1-m Equatorial Spread-F Irregularities and Plasma Bubbles," *J. Geophys. Res.*, **85:** 185, 1980b.

Tsunoda, R.T., "Backscatter Measurements of 11-cm Equatorial Spread-F Irregularities," *Geophys. Res., Lett.*, **7:** 848, 1980c.

Tsunoda, R.T., M.J. Baron, J. Owen, and D.M. Towle, "Altair: An Incoherent Scatter Radar for Equatorial Spread-F Studies," *Radio Sci.*, **14:** 1111, 1979.

Turco, R.P., "A Discussion of Possible Negative Ion Detachment Mechanisms in the Sunrise D Region," *Radio Sci.*, **9:** 655, 1974.

Untiedt, J., "A Model of the Equatorial Electrojet with a Meridional Current System," *J. Geophys. Res.*, **72:** 5799, 1967.

Vickrey, J.F., C.L. Rino, and T.A. Potemra, "Chatanika/TRIAD Observations of Unstable Ionization Enhancements in the Auroral F-Region," *Geophys. Res. Lett.*, **7:** 798–792, 1980.

Vondrak, R.R. and M.J. Baron, "Radar Measurements of the Latitudinal Variation of Auroral Ionization," *Radio Sci.*, **11:** 939–946, 1976; "A Method of Obtaining the Energy Distribution of Auroral Electrons from Incoherent Scatter Radar Measurements," *Radar Probing of the Auroral Plasma,* edited by A. Brekke, pp 315–330, Scandinavian University Books, Oslo, Norway, 1977.

Weber, E.J., J. Buchau, R.H. Eather, and R.S. Mende, "North-South Aligned Equatorial Airglow Depletions," *J. Geophys. Res.*, **83:** 712, 1978.

Weber, E.J., J. Buchau, and J.G. Moore, "Airborne Studies of F Layer Ionospheric Irregularities," *J. Geophys. Res.*, **85:** 4631, 1980.

Winningham, J.D. and W.J. Heikkila, "Polar Cap Auroral Electron Fluxes Observed with ISIS-I," *J. Geophys. Res.*, **79:** 949–958, 1974.

Woodman, R.F. and C. LaHoz, "Radar Observations of F Region Equatorial Irregularities," *J. Geophys. Res.*, **81:** 5447, 1976.

Woodman, R.F. and S. Basu, "Comparison Between in situ Spectral Measurements of Equatorial F Region Irregularities and Backscatter Observations at 3-m Wavelength," *Geophys. Res. Lett.*, **5:** 869, 1978.

Wright, J.N., "A Model of the F2 Region Above h_{max} F2," *J. Geophys. Res.*, **65:** 185, 1960.

Yeh, K.C., H. Soicher, and C.H. Liu, "Observations of Equatorial Ionospheric Bubbles by the Radio Propagation Method," *J. Geophys. Res.*, **84:** 6589, 1979.